



Measuring the seismic risk along the Nazca-Southamerican subduction front: Shannon entropy and mutability

2

3

4 Eugenio E. Vogel^{1,2}, Felipe G. Brevis¹, Denisse Pastén^{3,4}, Víctor Muñoz³,
5 Rodrigo A. Miranda^{5,6}, Abraham C.-L. Chian^{7,8}

6

7 ¹Departamento de Física, Universidad de La Frontera, Casilla 54-D, Temuco, Chile

8 ²Center for the Development of Nanoscience and Nanotechnology (CEDENNA), 9170124 Santiago, Chile

9 ³Departamento de Física, Facultad de Ciencias, Universidad de Chile, Santiago, Chile

10 ⁴Advanced Mining Technology Center (AMTC), Santiago, Chile

11 ⁵UnB-Gama Campus, University of Brasilia, Brasilia DF 70910-900, Brazil.

12 ⁶Plasma Physics Laboratory, Institute of Physics, University of Brasilia, Brasilia DF 70910-900, Brazil.

13 ⁷University of Adelaide, School of Mathematical Sciences, Adelaide, SA 5005, Australia.

14 ⁸National Institute for Space Research (INPE), Sao Jose dos Campos-SP 12227-010, Brazil

15

Correspondence to : eugenio.vogel@ufrontera.cl

16

17

18 **Abstract.** Four geographical zones are defined along the trench that is formed due to the subduction of the Nazca
19 Plate underneath the South American plate; they are denoted A, B, C and D from North to South; zones A, B
20 and D had a major earthquake after 2010 (Magnitude over 8.0), while zone C has not, thus offering a contrast for
21 comparison. For each zone a sequence of intervals between consecutive seisms with magnitudes ≥ 3.0 is set up and
22 then characterized by Shannon entropy and mutability. These methods show correlation after a major earthquake
23 in what is known as the aftershock regime, but show independence otherwise. Exponential adjustments for these
24 parameters reveal that mutability offers a wider range for the parameters characterizing the recovery compared to the
25 values of the parameters defining the background activity for each zone before a large earthquake. It is found that
26 the background activity is particularly high for zone A, still recovering for zone B, reaching values similar to those of
27 zone A in the case of zone C (without recent major earthquake) and oscillating around moderate values for zone D.
28 It is discussed how this can be an indication for more risk of an important future seism in the cases of zones A and
29 C. The similarities and differences between Shannon entropy and mutability are discussed and explained.

30

31

I. INTRODUCTION

32 A recent advance on information theory techniques, with the introduction of the concept of mutability (Vogel et al.,
33 2017), opens new ways of looking at the tectonic dynamics in subduction zones. The main goals of the present paper
34 are five-fold: 1) To establish the similarities and differences between mutability and the well-known Shannon entropy
35 to deal with seismic data distributions; 2) To find out which of the aforementioned parameters gives an advantageous
36 description of the subduction dynamics in order to discern different behaviors along the subduction trench; 3) To apply
37 this description to characterize the recovery regime after a major earthquake; 4) To use this approach to establish
38 background activity levels prior to major earthquakes; 5) To apply all of the above to different geographical zones
39 looking for possible indications for regions with indicators pointing for possible future major earthquakes.

40 Several statistical and numeric techniques have been proposed to analyze seismic events. For a recent review we
41 refer the interested reader to the paper by de Arcangelis et al. and references therein (de Arcangelis et al., 2016). We
42 shall concentrate here in the use of Shannon entropy and mutability which are introduced and discussed in the next
43 paragraphs; they will be applied to the intervals between consecutive seisms in each region.

44 Data may come from a variety of techniques used to record variations in some earth parameters like infrared
45 spectrum recorded by satellites (Zhang et al., 2019), earth surface displacements measured by Global Positioning
46 System (GPS) (Klein et al., 2018), variations of the earth magnetic field (Cordaro et al., 2018; Venegas-Aravena et
47 al., 2019), changes in the Seismic Electric Signals (Varotsos et al., 1984a) 1984b); Varotsos et al., 1986; Varotsos et
48 al., 1991; Varotsos et al., 1993; Varotsos, 2005; Sarlis et al., 2018; Varotsos et al., 2019), among others. In the present
49 work we make use of the seismic sequence itself analyzing the time intervals between filtered consecutive seisms.

50 Shannon entropy is a useful quantifier for assessing the information content of a complex system (Shannon, 1948). It
51 has been applied to study a variety of nonlinear dynamical phenomena such as magnetic systems, the rayleigh-Bernard
52 convection, 3D MHD model of plasmas, turbulence or seismic time series, among others (Crisanti et al., 1994; Xi et



53 al., 1995; Cakmur et al., 1997; Chian et al., 2010; Miranda et al., 2015; Manshour et al. 2009).

54 Analysis of the statistical mechanics of earthquakes can provide a physical rationale to the complex properties of
55 seismic data frequently observed (Vallianatos et al., 2016). A number of studies have shown that the complexity in the
56 content information of earthquakes can be elucidated by Shannon entropy. Telesca et al. (Telesca et al., 2004) applied
57 Shannon entropy to study the 1983-2003 seismicity of Central Italy by comparing the full and the aftershock-depleted
58 catalogues, and found a clear anomalous behaviour in stronger events, which is more evident in the full catalogue
59 than in the aftershock-depleted one. De Santis et al. (De Santis et al., 2011) used Shannon entropy to interpret the
60 physical meaning of the parameter b of the Gutenberg-Richter law that provides a cumulative frequency-magnitude
61 relation for the statistics of the earthquake occurrence. Telesca et al. (Telesca et al., 2012) studied the interevent-time
62 and interevent-distance series of seismic events in Egypt from 2004 to 2010, by varying the depth and the magnitude
63 thresholds.

64 Telesca et al. (Telesca et al., 2013) combined the measures of the Shannon entropy power and the Fisher information
65 measure to distinguish tsunamigenic and non-tsunamigenic earthquakes in a sample of major earthquakes. Telesca
66 et al. (Telesca et al., 2014) applied the Fisher-Shannon method to confirm the correlation between the properties of
67 the geoelectrical signals and crust deformation in three sites in Taiwan. Nicolis et al. (Nicolis et al., 2015) adopted
68 a combined Shannon entropy and wavelet-based approach to measure the spatial heterogeneity and complexity of
69 spatial point patterns for a catalogue of earthquake events in Chile.

70 In the last two decades the concept of "natural time" for the study of earthquakes has been introduced by Varotsos
71 et al. (Varotsos et al., 1984; Varotsos et al. 1991; Varotsos et al. 1993; Varotsos et al., 2011) This method proposes a
72 scaling of the time in a time series, by using the index $\chi_k = k/N$, where k indicates the occurrence of the k -th event
73 and N is the total number of the events in a time series. For example, for seismic time series the evolution of the
74 pair (χ_k, M_{0k}) is following, where M_{0k} is proportional to the energy released in an earthquake, finding interesting
75 results in the Seismic Electric Signal previous to an earthquake occurrence (Sarlis et al., 2013; Sarlis et al., 2015;
76 Sarlis et al., 2018a); Sarlis et al. 2018b); Rundle et al., 2018). An entropy could be defined in natural time by
77 $S \equiv \langle \chi \ln(\chi) \rangle - \langle \chi \rangle \ln \langle \chi \rangle$, and has been very useful in the analysis of global seismicity (Rundle et al., 2019).

78 Bressan et al. (Bressan et al., 2017) used Shannon entropy and fractal dimension to analyze seismic time series
79 before and after eight moderate earthquakes in Northern Italy and Western Slovenia.

80 On the other hand, the method based on information theory (Luenberg, 2006; Cover et al., 2006; Roederer 2005)
81 was introduced a decade ago when it was successfully used to detect phase transitions in magnetism (Vogel et al.,
82 2009; Vogel et al., 2012; Cortez et al., 2014). Then a new data compressor was designed to recognize compatible data,
83 namely, data based on specific properties of the system. This method required comparing strings of fixed length and
84 starting always at the same position within the digits defining the stored record. For this reason it was named "word
85 length zipper" (wzip for short) (Vogel et al., 2012). The successful application of wzip to the 3D Edwards-Anderson
86 model came immediately afterwards, where one highlight was the confirmation of a reentrant transition that is elusive
87 for some of the other methods (Cortez et al., 2014). Another successful application to critical phenomena was for the
88 disorder to nematic transition that occurs for the depositions of rods of length k (in lattice units) on square lattices:
89 for $k \geq 7$ one specific direction for depositions dominates over when deposition concentration overcomes a critical
90 minimum value (Vogel et al., 2017).

91 But wzip proved to be useful not only for the case of phase transitions. It has been used in less drastic data
92 evolution revealing different regimes or behaviors for a variety of systems. The first of such applications were in
93 econophysics dealing with stock markets (Vogel et al., 2014) and pension systems (Vogel et al., 2015). The alteration
94 of the blood pressure parameters was also investigated using wzip (Contreras et al., 2016). At a completely different
95 time scale the time series involved in wind energy production in Germany was investigated by wzip yielded recognition
96 of favorable periods for wind energy (Vogel et al., 2018)

97 The first application of wzip to seismology came recently using data from a Chilean catalogue finding that wzip
98 results clearly increase several months prior to large earthquakes (Vogel et al., 2017). The main point in that paper
99 was to establish the method without attempting further analyses or comparison with other methods or to compare
100 possible seismic risk among regions.

101 In the present paper we make a new analysis comparing results from mutability and Shannon entropy applied to
102 data of seismic data along the subduction front parallel to the Chilean coast. The complete tectonic context shows
103 an active and complex seismic region for all the coast, driven by the convergence of the Nazca plate and the South
104 American plate, at a rate of 68 mm yr^{-1} (Altamimi et al., 2007) approximately. In the last 100 years, many large
105 earthquakes have been localized in the shock between these two plates, such as Valparaíso 1906 ($M_w=8.2$), Valdivia
106 1960 ($M_w=9.6$), Cobquecura 2010 ($M_w = 8.8$), Iquique 2014 ($M_w=8.2$), and Illapel 2015 ($M_w =8.4$). So, this zone
107 is an attractive source for studying seismic activity associated to large earthquakes. But although the dynamics
108 along the Chilean coast may be dominated by the interaction between these two plates, various works have pointed
109 out variations along the coast which may yield information about the details of that interaction. For instance, the
110 coupling between these two plates has been studied by Metois et al. (Metois et al., 2012; Metois et al. 2013) in the



111 last years, concluding that the subduction area has alternated zones of high an low coupling (Metois et al., 2012;
 112 Metois et al., 2013). This suggests that it is interesting to apply novel nonlinear techniques to study such variability.
 113 Here, we propose new ways to characterize some of the various dynamics that may be present along the subduction
 114 zone in this trench. In order to do that, we will consider four regions along the coast of Chile characterizing them
 115 mainly by their latitudes.

116 The paper is organized in the following way. Next Section is about methodology dealing with the data and
 117 parameters to be measured. Section 3 presents the results discussing them and comparing the alternative methods.
 118 Last Section is devoted to conclusions.

119 II. METHODOLOGY

120 A. Data organization

121 Earthquakes originated in the subduction zone of the Nazca plate underneath the South American plate have been
 122 recorded, interpreted and stored in several data seismic data banks. In the present study we shall use the data
 123 collected by the Chilean National Seismic Centre (Centro Sismológico Nacional: CNS) (Web, 2019), which are very
 124 accurate regarding the location of the epicenters. In particular, we have used a seismic data set collected from March
 125 2005 until March 2017, containing 22 697 events, distributed along the coast of Chile, from Arica in the far north up
 126 to Temuco in the south of Chile. These data are freely available through CNS (www.sismologia.cl).

127 In order to analyze the spatial evolution of the mutability and Shannon entropy along this part of the subduction
 128 zone, we have focused our attention on four regions defined below. For each region we have corroborated that the
 129 Gutenberg-Richter law holds, finding a common completeness magnitude of $M_w = 3.0$. Thus, all the following analysis
 130 will be made using only the seismic events with magnitudes of at least $M_w = 3.0$. We have considered seismic data
 131 sequences for four specific geographical zones: three of them include one earthquake over 8.0 occurring after 2010,
 132 and we have added for comparison a neighboring area with no such large earthquake during several recent years.

133 Starting from the North, the zones are the following: A) around the earthquake near Iquique (2014; $M_w = 8.2$)
 134 including 6891 events; B) around the earthquake near Illapel (2015; $M_w = 8.4$) including 6626 events, C) a quieter
 135 geographical region (calm zone) at the center of Chile (where the greatest seismic event is $M_w = 6.5$), including 2824
 136 events; and D) around the earthquake in Cobquecura (2010, $M_w = 8.8$) including 6356 events. The observation time is
 137 from January 1, 2011 to March 23, 2017 for zones A, B and C, while it is from January 1, 2009 to March 23, 2017 for
 138 zone D (no special reason for this last date). We extended the analysis in the case of zone D to include the regime
 139 previous to the big earthquake of 2010. Since the analysis is either relative to the size of the sample or dynamical
 140 along the series this difference should not affect the discussion below.

141 All zones have a similar geographical extension with some singularities that we explain here. Regions A,B, and D
 142 have latitudes centered at the epicenter of the largest earthquake of each zone; the span in longitude is the same for
 143 these zones. zone A misses the 4.0° spans in latitude of zones B and D, since the Chilean catalogue ends at -17.926°
 144 which is the northern limit for this zone (for homogeneity of the data we do not mix catalogues). On the other hand,
 145 zone C was chosen to include a populated area of the country but with no earthquake over 8.0 and showing less
 146 important activity than previous ones. Details are given in Table I, and are illustrated in Fig. 1. As it can be seen in
 147 this map zone C overlaps with both B and D: to avoid getting close to the epicenter of the main earthquake in zone
 148 D, zone C was shortened in its South extension. So the data catalogues have been filtered by latitude, longitude and
 149 magnitude. At this point we do not filter by depth which should not greatly influence the comparison among zones
 150 since it is a common criteria for all of them.

Zone	Latitudes		Longitudes		Main Earthquake			
	N	S	W	E	Magn	Y	M	D
A	-17.926°	-21.572°	-75.00°	-68.00°	8.2	2014	4	1
B	-29.637°	-33.637°	-75.00°	-68.00°	8.4	2015	9	16
C	-32.700°	-35.500°	-74.00°	-69.00°	(6.5)	2012	4	17
D	-34.290°	-38.290°	-75.00°	-68.00°	8.8	2010	2	27

TABLE I. Geographical definition of the 4 zones considered in this study. The strongest seismic event in each zone is identified at the end. zone C lacks a very strong seism during recent years which is indicated by the use of parenthesis for the strongest seism here. The geographical coordinates and time windows are explained and defined in the text.

151 For all seismic events characterized above we calculate the interval in minutes (rounding off seconds) between
 152 consecutive events. Then a vector file is produced storing the consecutive intervals between theses seisms within each

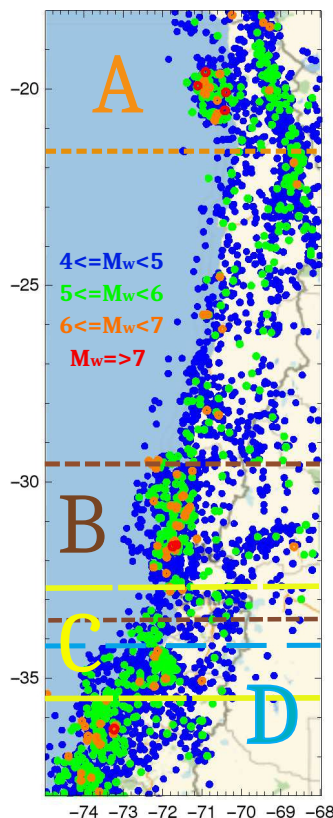


FIG. 1. Map showing the seismic events with magnitudes greater than M_w 4.0 and the division in four geographical zones A, B, C, and D defined in Table I. The seismic events are shown by circles using the following color code according to magnitude: between 4.0 and 4.9 in blue, between 5.0 and 5.9 in green, between 6.0 and 6.9 in orange, and for magnitude equal or greater than M_w 7.0 in red.

153 zone. These are the files to be analyzed by Shannon entropy and mutability. Notice that there is a close similarity
154 between this and the “natural time” analysis discussed in the Introduction, since the resulting vector is indexed by
155 the event number. However, in our case the value of each vector component is the interevent time itself, thus temporal
156 information is still kept in the time series.

157 Let us consider histograms for interval distributions for each zone with consecutive bins of 60 minutes each. Per-
158 centage of abundance $G_{K,i}$ of intervals are obtained for the i -th bin for the different zones Z : A, B, C, or D. Figure 2
159 shows the histograms corresponding to the distribution functions $G_{Z,i}$. It can be immediately seen that shorter inter-
160 vals have been more frequent in zones D and B, while they are less frequent in the C zone. Zone A presents and
161 intermediate presence of small intervals. This different frequency for small seisms finds an explanation in the presence
162 of large earthquakes in B and D followed by large aftershock periods, while in zone A the aftershock period (and
163 the number of short intervals) was very short as we will see in detail below; zone C does not include any aftershock
164 period so short intervals are less frequent here. These plots are presented in a semilog scale to better appreciate any
165 possible decay law. However, no general behavior is found evidencing the different dynamics among the zones. Zone
166 A presents a linear decay in this scale while zone C is the more irregular one. On the other hand, zone D departs
167 quite clearly from a linear dependence evidencing the lack of saturation several years after the huge earthquake of
168 2010. Scaling algorithms have been suggested to deal with the time series on the interevent sequence (Lippiello et al.
169 2012) but in the present study we leave the series with the natural interevent intervals to analyze them by means of
170 information theory as proposed below.

171 We can increase the precision of the data treatment below by the use of a database providing more positions for the
172 numeric recognition (Vogel et al., 2017). This was achieved by choosing a numerical basis providing more positions
173 to be matched. So the data files used both for Shannon entropy and for mutability used digits corresponding to a

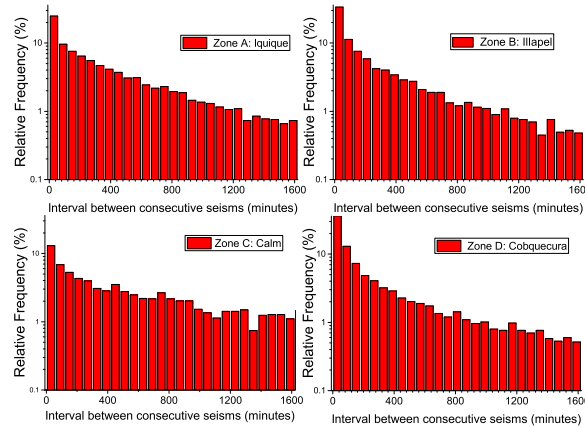


FIG. 2. Distribution functions $G_{Z,i}$ ($Z = \{A, B, C, D\}$) for intervals between two consecutive seismic events.

174 quaternary numerical basis.

175

B. Shannon entropy

176 Let Δ_i , $i = 1, \dots, N$ be the full sequence of time intervals between consecutive seisms in any of the already defined
 177 zones. The time that the i -th event occurred can be obtained by $t_i = t_0 + \sum_{j=1}^i \Delta_j$, where t_0 is the start time of the
 178 dataset. The Shannon entropy for Δ_i within a sliding window of size ν events can be calculated as follows

$$H(t_i, \nu) = - \sum_{j=i}^{i+\nu} p_j \ln(p_j) \quad (1)$$

179 where p_j is the probability distribution function of the time intervals within the time window, which can be determined
 180 by constructing a normalized histogram

$$p_j = g_j / \nu \quad (2)$$

181 where g_j is the number of times Δ_j occurs within the sliding window. The appropriate value for ν depends on the
 182 kind of data under consideration. Thus, for instance, application to this method to the minute variations of the
 183 stock market yielded $\nu = 30$ (half-an-hour) as a significant time window to establish tendencies in this economical
 184 activity (Vogel et. al 2014). In the case of seismic sequences ordered by real time, time windows between $\nu = 24$ and
 185 $\nu = 96$ were investigated finding that $\nu = 24$ is appropriate to deal with seismic activity (Vogel et. al 2017). More
 186 details about the choice of ν can be found in these references in particular in Fig. 3 of the last reference. So, for all
 187 applications below we use $\nu = 24$.

188

C. Data recognizer

189 We use here the same dynamical data window of ν events used for the calculation of Shannon entropy. The weight
 190 in bytes of the sequence of ν events beginning at natural time i will be denoted by $w(t_i, \nu)$. This partial sequence is
 191 processed by wzip producing a new sequence that needs $w^*(t_i, \nu)$ bytes of storage. The relative dynamic information
 192 content of this time series of seismic events is known as mutability, which is defined as



$$\mu(t_i, \nu) = \frac{w^*(t_i, \nu)}{w(t_i, \nu)}, \quad (3)$$

193 where w^* is the size in bytes of the compressed dataset associated to the time intervals Δ_j within the time window
 194 of ν events.

195 As already pointed out $\nu = 24$ for all mutability calculations below. The typical value of $w(t_i, \nu)$ for the files
 196 measured here is 144 bytes, while the values of $w^*(t_i, \nu)$ vary roughly between 100 to 400 bytes thus leading to
 197 variations in mutability. To better illustrate this concept we include an Appendix calculating the mutability for 4
 198 different sequences of 24 events.

199 Two comments are in order: First, wzip uses compressor algorithms to recognize information but this does not
 200 mean that $w^*(t_i, \nu)$ should be less than $w(t_i, \nu)$; Second, the value of wzip depends both on the interval distribution
 201 but also on the time sequence of the intervals while Shannon entropy depends only on the distribution. Thus, the
 202 sooner a value in the sequence is repeated, the lower the value of $\mu(t_i, \nu)$ is (Vogel et al., 2012; Cortez et al., 2014).
 203 This fact marks a difference between these two parameters as we will see below.

204

III. RESULTS

205 Figs. 3, 4, 5 and 6 present the Shannon entropy (top) and mutability (bottom) for data corresponding to geograph-
 206 ical areas A, B, C and D respectively according to Table I and Fig. 1. The numeric recognition was done for the data
 207 files (intervals in minutes between successive seisms) in quaternary basis both for Shannon entropy and mutability.
 208 All registers have the same number of digits filling with zeroes all empty positions previous to first significant digit,
 209 The matching to recognize the same data register started at position 4 and was done for three digits including the
 210 fourth position (Vogel et al., 2017). All zones were treated with the same precision.

211 In the upper panel the abscissa "Time" corresponds to real time t_i (as defined in Section II. B) beginning on January
 212 1, 2011 for zones A, B and C, or on January 1, 2009 for zone D. In the lower panel the abscissa labelled "Events"
 213 corresponds now to the succession of filtered seisms identified by the same label i used to define t_i . The ordinates are
 214 the same in both panels.

215 In the upper panel the aftershock behavior is concealed by the large activity in the short time after a large quake,
 216 while in the lower panel it is easier to see the aftershock sequence although the large quiet periods look now more
 217 compressed. Earthquakes over a certain magnitude (as given in the inset for each zone) are marked by a star. The
 218 empty square (A, B, and D only) identifies the largest earthquake with magnitude greater than $M_w = 8.0$ within that
 219 area as listed in Table I.

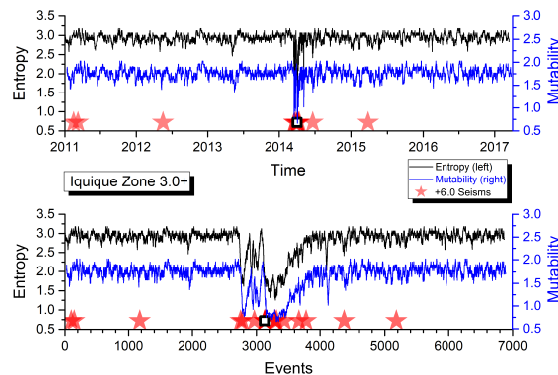


FIG. 3. Shannon entropy and mutability as functions of the sequence of events for the seismic activity of the A zone. The open star marks the position of the earthquake identified in Table I. The abscissa in the upper panel corresponds to real time t_i while in the lower panel it represents the successive events (filtered seisms) denoted by the order label i (Figs. 4, 5, and 6 use the same procedure).

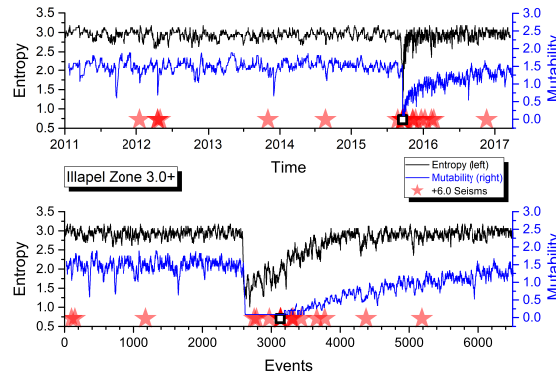


FIG. 4. Shannon entropy and mutability as functions of the sequence of events for the seismic activity of the B zone. The open star marks the position of the earthquake identified in Table I.

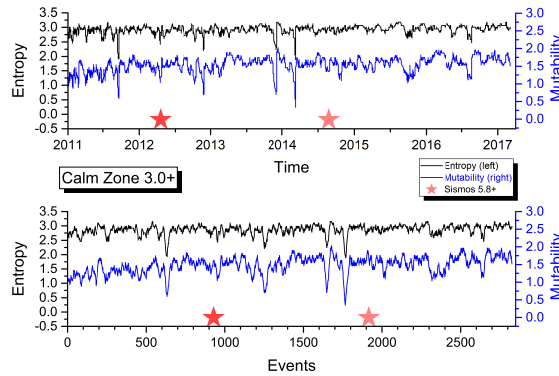


FIG. 5. Shannon entropy and mutability as functions of the sequence of events for the seismic activity of the C zone.

220 As it can be observed, both H and μ present a similar behavior for the data in the four areas. Immediately
 221 after a large shock both indicators sharply decrease due to the short intervals between consecutive aftershock quakes
 222 thereafter.

223 The average activity level is relatively constant before a major earthquake and later on after the aftershocks have
 224 disappeared. However, such activity level is not the same for all the areas which is an indication of different response
 225 to similar phenomena which deserves particular attention and it will be further investigated below.

226 To better appreciate the correlation between H and μ we study the out-of-phase correlations defined as

$$C_H(\ell) = \frac{1}{(N - 2m - 1)\sigma_H\sigma_\mu} \sum_{i=m+1}^{i=N-m} [H(i) - \bar{H}][\mu(i - \ell) - \bar{\mu}] \quad (4)$$

$$C_\mu(\ell) = \frac{1}{(N - 2m - 1)\sigma_H\sigma_\mu} \sum_{i=m+1}^{i=N-m} [H(i - \ell) - \bar{H}][\mu(i) - \bar{\mu}] \quad (5)$$

227 where ℓ is the phase difference measured in terms of number of events separating the measurement of one parameter
 228 with respect to the other and $m = 50$ is the range or maximum phase difference in either sense considered here. This
 229 value is entirely empirical looking for a flat behavior of previously defined correlations. From Fig. 7 it may appear

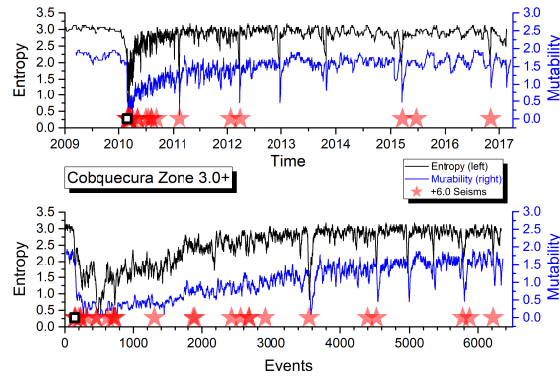


FIG. 6. Shannon entropy and mutability as functions of the sequence of events for the seismic activity of the D zone. The open star marks the position of the earthquake identified in Table I.

230 that $m = 30$ could be enough but we decided to explore a bit further to make sure curves are already tending to a
 231 flat behavior. Previous equations represent the average over the $(N - 2m - 1)$ possible equivalent ranges within the
 232 series on N registers. In addition σ_H and σ_μ represent the standard deviations of H and μ through the N events
 233 respectively.

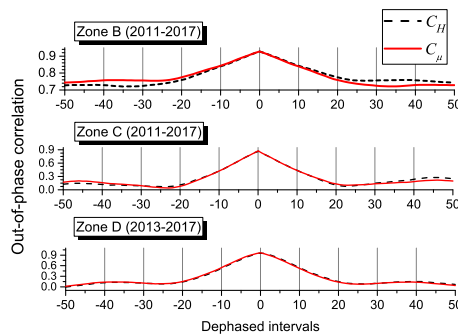


FIG. 7. Out-of-phase correlations. Upper panel: B zone data including aftershock regime (similar ones are obtained for zones A and D with aftershock regimes). Middle panel: C zone data that does not present aftershock regime. Lower panel: Truncated D zone data to exclude the aftershock regime.

234 The out-of-phase correlation between Shannon entropy and mutability is presented in Fig. 7: it was found that in
 235 general full correlation is lost after about 20 events. A general prevalence is observed in the form of a tendency towards
 236 a constant behavior far from the maximum: a value around 0.75 in the wings of zone B (top panel) and towards 0.15
 237 for the zone C (middle panel). Similar figures were analyzed for zones A and D with prevalence values near 0.75
 238 and 0.57 respectively. To test if these prevalence correlations are due to the aftershock regimes a reevaluation of the
 239 out-of-phase correlation was done for the D zone restricted to results of Shannon entropy and mutability obtained
 240 after January 1, 2013, thus diminishing the effect of the aftershock regime; these results are also shown in Fig. 7 (lower
 241 panel). So the main correlation between Shannon entropy and mutability is obtained during the aftershock period.
 242 On the other hand the out-of-phase correlation tend to be completely lost during periods without the influence of this
 243 regime. This is a first indication for partial independence between Shannon entropy and mutability.

244 The recovery of the activity level after a major earthquake is faster for the Shannon entropy than for the mutability.
 245 Namely, the slope in the recovery for μ is better defined after a large quake. It is interesting to notice from figures 3
 246 through 6 that zone A recovered its foreshock activity level sooner than any of the other zones. This observation will
 247 be put in a quantitative way concentrating on the recovery dynamics in real time to compare the behavior of the



248 different zones.

249 Figure 8 presents the mutability results for region D starting at the point of minimum mutability occurring
 250 immediately after the major earthquake on February 27, 2010. The dotted (red) curve corresponds to an exponential
 251 fit to be discussed next. The inset shows the same data and exponential adjustment for the first two years on the
 252 time span. A power law can be seen at the onset of the aftershock regime resembling Omori's law.

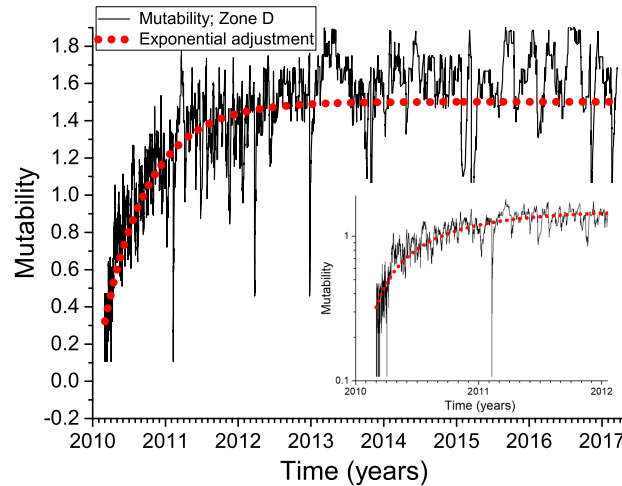


FIG. 8. Exponential fit for Cobquecura data set after February 27, 2010. This data set starts at the point of minimum mutability after the big earthquake of magnitude $M_w = 8.8$.

253 For zones A, B, and D, we assume an exponential adjustment for the mutability function after the largest earthquake.
 254 A possible such function is:

$$\mu_{eZ}(t) = a_Z + b_Z \exp(-(t - t_Z)/\tau_Z), \quad (6)$$

255 where a_Z measures the “asymptotic” activity of zone Z (reached after the aftershocks regime), t_Z corresponds to the
 256 time of minimum mutability after the largest earthquake (Table I) and serves as initial time for this recovery analysis;
 257 τ_Z is the characteristic time for activity recovery in zone Z . b_Z is just a shape adjustment parameter without a direct
 258 meaning for this analysis.

259 For zone D (Fig. 8), the best least square fit for the mutability is obtained for $a_D = 1.502(2)$ and $\tau_D = 0.62212$ years
 260 (y). The results of this treatment for all the zones with major earthquakes are summarized in Table II. Fig. 8 includes
 261 an inset with semilog scale to appreciate the recovery process under a different perspective. A linear behavior in this
 262 scale is insinuated at the beginning of the plot, but then it is rapidly lost. The sudden decrease of mutability values
 263 during February 2011 is better resolved in the time scale of the inset: this is due to the short aftershock activity
 264 produced by an earthquake of magnitude 6.1 occurred on February 14, 2011. Due to their sharp appearance we
 265 propose to call “needles” these sudden and short decreases of mutability associated to the brief aftershock period left
 266 by seisms M5.0 to M6.0 approximately. Other needles can be easily spotted in Figs. 3, 4, 5, 6 and 8.

Zone Z	a_Z	b_Z	t_Z (y)	τ_Z (y)
A	1.754 (0.002)	-1.64691	2014.24829	0.0134(3)
B	1.208 (0.004)	-1.09124	2015.70784	0.2092(33)
D	1.502 (0.005)	-1.37833	2010.07093	0.6221(110)

TABLE II. Best fit parameters for the mutability of zones A, B, and D, after the main earthquake, using the exponential trial function given by Eq. (6).

267 A similar analysis was made for the Shannon entropy results using the same exponential fit and the corresponding
 268 parameters are given in Table III.



Zone Z	a_Z	b_Z	t_Z (y)	τ_Z (y)
A	2.924(2)	-3.69218	2014.24516	0.0095(3)
B	2.908(3)	-2.30957	2015.69997	0.0246(4)
D	2.815(4)	-2.29226	2010.13133	0.1255(25)

TABLE III. Best fit parameters for Shannon entropy of zones A, B, and D, after the main earthquake, using the exponential trial function Eq. (6).

269 Figures similar to Fig. 8 were made for the mutability of zones A and B using the best fit parameters listed
270 in Table II. The same analysis was also done for the results obtained by Shannon entropy and the corresponding
271 parameters are given in Table III. The figures backing such fittings are not included here since they are very similar
272 to Fig. 8 and the procedure is the same to the one already established in the presentation of this figure.

273 Let us now discuss the results given in Tables II and III which list the parameters defined in Eq. 6. The first
274 striking difference between Shannon entropy and mutability is on the value for the background parameter a_Z . In
275 the case of the adjustment for Shannon entropy this parameter does not discriminate significantly among zones with
276 values close to 2.9 for all of them; the same parameter in the case of the mutability data spans a range [1.208,1.754],
277 thus indicating differences in the dynamics of these three regions. In particular, mutability indicates that in zone B
278 there are more seismic events at regular intervals than in the other zones. Given the underlying plate subduction
279 mechanism, this could mean that plates are sliding more regularly or even fluently in zone B, whereas the relative
280 motion of the Nazca plate under the South-American plate is more difficult in zone A, thus leading to more disperse
281 set of intervals between consecutive seisms.

282 After a large earthquake the zones tend to recover their characteristic activity level a_Z , but this is done rather
283 abruptly for Shannon entropy while it is more gradual for mutability. This is measured by the recovery time τ_Z in
284 Tables II and III. In the case of the Shannon entropy for the zone A the recovery is very fast, namely 0.00947 years
285 \approx 3.5 days. In the case of zones B and D the recovery times for the Shannon entropy are of 9 days and 45 days,
286 respectively. However, when the analysis is done using the recovery time for mutability (Table II) the recovery times
287 are 5 days, 2.5 months and 7.5 months for the zones A, B, and D, respectively.

288 Tables II and III also show that recovery times τ_Z are different, shorter for Shannon entropy and longer for
289 mutability, but the tendencies are the same. So eventually both methods can be used to characterize this aspect of
290 the aftershock regime. In terms of the human perception experienced after any large earthquake it seems that τ_Z
291 values obtained for the mutability results are more representative of the aftershock times experienced in each zone.
292 Thus, for instance, seisms of magnitude around 4.0 were frequent in zone D during several months after February 10,
293 2010, but this was not the case for zone A where people lost perception of the aftershock regime after a week or so of
294 the last earthquake in this area.

295 The main difference between Shannon entropy and mutability is that the former analyzes the distribution of registers
296 in a sequence regardless of the order in which these entries were obtained, while the latter gives a lower result for
297 sequences including frequently repeated registers (Cortez et al., 2014). Shannon entropy considers the visit to a state
298 without considering the order in which these visits take place, so it pays exclusive attention to the probability of
299 visiting a state at some instance during the observation time. Mutability considers also the trajectory in which these
300 visits take place, giving lower results when the system stays long periods in the same state or states directly connected
301 to this state; on the contrary during agitated periods (chaotic regimes would be at the apex here) mutability gives
302 higher results. In other words, a given sequence has just one result for Shannon entropy but the permutations of the
303 order of the registers lead to different results for mutability; in the present case the mutability results reported here
304 corresponds to the natural sequence of the recorded seisms.

305 We now focus on the analysis of the background activity obtained for the 4 zones described in this work, taking
306 semestral averages of the values of mutability in Figs. 3–6, in order to study trends in time scales longer than the
307 one of previous figures. We have chosen a semester as the time for averages so we have a few hundreds registers in
308 each partial sequence minimizing error, but still we have some 13 points in the overall period to appreciate tendencies
309 and differences. In doing so, we also evaluate semestral averages of intervals between consecutive seisms, which show
310 similar trends to the mutability results for the same period.

311 The semestral analysis for zones A, B, C and D is shown in Figs. 9, 10, 11 and 12, respectively; they are all
312 presented under the same scale to allow a direct comparison. The mutability values run on the upper part (black)
313 while the intervals tend to occupy the lower part (blue) of the plot. The first comment here is evident: these 4
314 regions present different seismic behaviors so we have to discuss them separately. The only common feature is that an
315 earthquake with magnitude over 8.0 produces an absolute minimum for both variables during the semester containing
316 this seism and its aftershock sequence.

317 For didactical reasons we shall perform this discussion beginning with zone D, where the long recovery period
318 already appreciated in Fig. 6 and in Table II is more enhanced. It is interesting to observe that the average semestral



319 mutability presents recent relaxations like in the first semester of 2015 and the first semester of 2017. Generally
320 speaking these results do not approach yet the values near 1.8 for the average semestral mutability in the foreshock
321 period preceding the large earthquake of 2010. Interval semestral averages tend to follow the variations of mutability
322 but some differences are noticed. The present average interval of about 2000 minutes (about 33 hours) is far from the
323 almost 6000 minute interval before the large earthquake.

324 Fig. 11 is completely different to the others. There is no major earthquake included here but it is obvious that there
325 was one prior to 2011 from which this activity is slowly recovering. The general tendency is to slowly increase the
326 mutability values to levels similar to those constantly presented by zone A and those presented by region D previous
327 to the large earthquake. Interval averages also increase reaching just under 2000 minutes. If this is an announcement
328 for a future major earthquake in zone C or nearby is still too early to tell but this zone should be monitored closely.

329 Fig. 10 shows the foreshock mutability averages for zone B which present a nearly flat behavior around 1.6 before
330 the major earthquake of 2015. Then, after the aftershock regime the average semestral mutability begins to recover,
331 faster than in zone D, but still not reaching the level shown here previous to the large earthquake. The observation
332 is similar for the interval semestral average whose value is still small compared to the activity before 2016.

333 Fig. 9 shows the almost constant results (near 1.8) for the average semestral mutability of zone A, with just one
334 semester reaching a moderate low value (1.4 with large error bar). The semestral average for intervals between seisms
335 is also rather flat around 10 hours. The only exception is the first semester of 2014 in coincidence with the large
336 earthquake there.

337 Error bars deserve a separate discussion. They are obtained from the standard deviations calculated for the
338 distributions of each semester within each zone. So the number of events differ from one semester to another even
339 within each zone. In the case of intervals the largest semestral error is of 4966 minutes for zone D during the second
340 semester of 2009, just prior to the large earthquake of 2010. The smallest error is of 280 minutes obtained for the
341 first semester of 2014, which includes the large earthquake and related activity in zone A. In the case of mutability
342 its largest semestral error is for zone A during the first semester of 2014, while the smallest one is during the second
343 semester of 2013 for this same zone. So error bars are subject to some fluctuations also but still they are a general
344 indication for the homogeneity of the data.

345 Mutability error bars are rather small for the A zone, meaning that the intervals are rather similar along the data
346 sequence. This is reinforced by the average interval error bars which are the smallest among the four zones (spanning
347 only about 1200 minutes) telling that intervals are not so different among themselves. The largest error bars both for
348 mutability and intervals are to be found in zone D; moreover they are irregular in recent years. Error bars increased for
349 the average in zone D during 2009 just prior to the huge quake of 2010. However, for this same zone the corresponding
350 error bars for the average semestral mutability are among the smallest to be found prior to this large earthquake. Once
351 again it is difficult to say something about the present status of zone B since it is clearly under recovery. However,
352 the Calm zone C is clearly showing a tendency: error bars for mutability averages are shrinking, while error bars for
353 intervals are growing spanning about 60 hours. These two symptoms were present in zones A, B and D previous to
354 their large respective earthquakes. In the case of zone A the error bars for the average intervals are not so large, but
355 here is where we find the highest values for mutability and the smallest error bars for this variable.

356 If we look for common features just before a large earthquake they are: relatively high mutability values ("high"
357 needs to be defined for each zone) and very small error bars associated with semestral mutability averages. The
358 particular values of these indicators for zone A could be interpreted as an irregular subduction here, with no short-
359 time accommodations or lack of fluency, leading to seismic risk of some sort, although it is not possible to specify
360 any possible time for a large seism in the future. From this point of view, the earthquake of 2014 near Iquique was
361 just a small accommodation of the plates but the subduction process could be somewhat stuck to the similar levels
362 presented before the large quake.

363

IV. CONCLUSIONS

364 Seismic activity is different for the four zones defined here along the Nazca-South American subduction trench (Figs.
365 1-2, Table I). Nevertheless, some general behaviors are common to the seismicity of the tectonic activity present in
366 this region. Both Shannon entropy and mutability show a sudden decrease after an earthquake of magnitude around
367 or over 7.0 (Figs. 3-6). Additionally, Shannon entropy and mutability reach "high" values before a major earthquake;
368 the scale to define "high" needs to be tuned for each geographical region and observation time window.

369 A short time correlation exists between Shannon entropy and mutability during the aftershock regime. However,
370 this correlation is lost far from this regime thus providing independent tests to characterize the seismic activity (Fig.
371 7).

372 The aftershock regime is characterized by successions of low and medium intensity seisms at short intervals producing
373 low values of both Shannon entropy and mutability. After some recovery time the intervals tend to go back to the kind

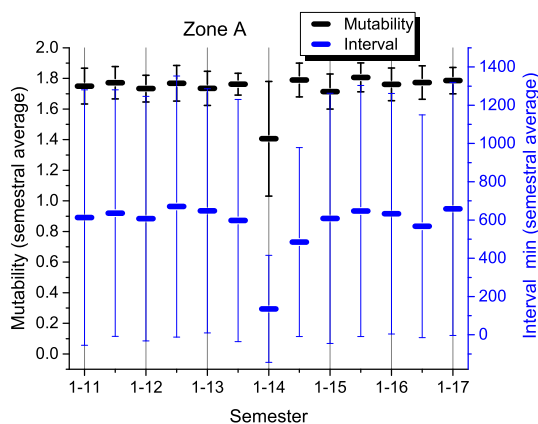


FIG. 9. Semestral average of mutability values (upper symbols; black) and intervals in minutes between consecutive seisms (lower symbols; blue) for zone A: Iquique. Odd semesters are labeled on the abscissa axis (1-13: first semester of 2013) while even semesters are only marked.

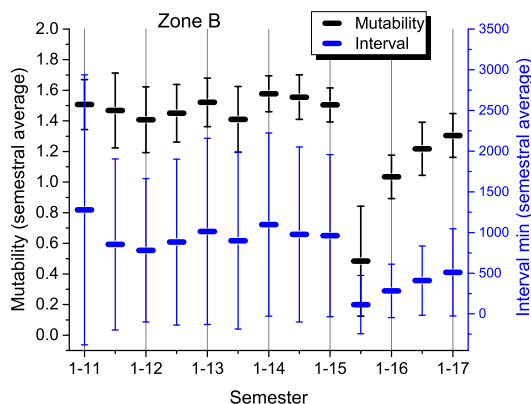


FIG. 10. Semestral average of mutability values (upper symbols; black) and intervals in minutes between consecutive seisms (lower symbols; blue) for zone B: Illapel. Odd semesters are labeled on the abscissa axis (1-13: first semester of 2013) while even semesters are only marked.

374 of intervals present before the large quake. This recovery behavior can be described by exponential adjustments (Fig.
 375 8) which indicate that the characteristic times are longer for mutability than for Shannon entropy (Tables II-III);
 376 eventually this speaks in favor of the former to continue the analysis. Another advantage of mutability is that the
 377 parameter reflecting the background activity span larger ranges than the one presented by the adjustment of Shannon
 378 entropy (Tables II-III). From these results the mutability recovery time τ_Z for zone A lasted a few days, while the
 379 same parameters for zone D lasted several months, which is close to the human perception in these zones.

380 The differences between Shannon entropy and mutability evidenced after the recovery time are due to the handling
 381 of a static distribution by the former while the latter considers exact or approximate repetitions in the data chain.
 382 From this point of view mutability carries more information than Shannon entropy in spite both are obtained from
 383 the same natural time sequences.

384 The background activity based on mutability a_Z (Tables II-III) is quite different for each zone (Figs. 9-12). This
 385 means that the subduction process finds different difficulties in each zone. However, some general features describing
 386 the motion of the Nazca plate under the South-American plate should be present along the trench. To investigate

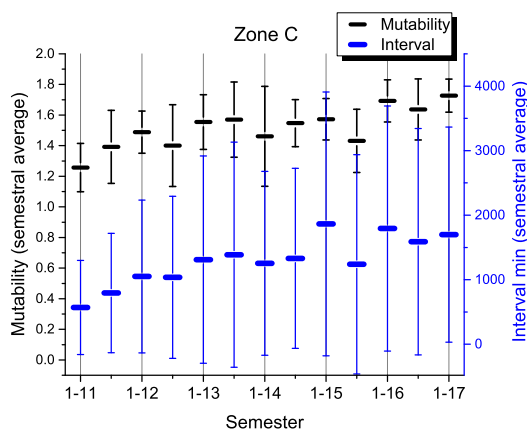


FIG. 11. Semestral average of mutability values (upper symbols; black) and intervals in minutes between consecutive seisms (lower symbols; blue) for zone C: Calm. Odd semesters are labeled on the abscissa axis (1-13: first semester of 2013) while even semesters are only marked.

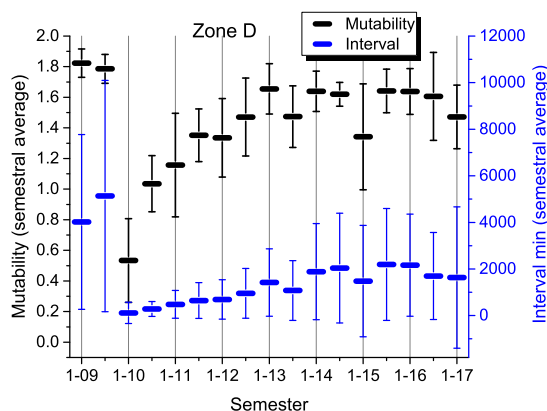


FIG. 12. Semestral average of mutability values (upper symbols; black) and intervals in minutes between consecutive seisms (lower symbols; blue) for zone D: Cobquecura. Odd semesters are labeled on the abscissa axis (1-13: first semester of 2013) while even semesters are only marked.

387 this possibility we considered semestral averages of mutability values.

388 Semestral averages for mutability recovered soon for zone A after the 8.2 earthquake, which indicates that the
389 short intervals after a major earthquake were mostly absent here. Soon, the regime with longer and different intervals
390 reappeared raising the values of mutability and narrowing the corresponding error bars; this could be interpreted as
391 a warning for a possible earthquake in this zone sometime in the near future. On the opposite side is zone D where
392 the semestral averages still do not recover to the levels prior to the large 8.8 earthquake of 2010; moreover, there have
393 been instances lowering the semestral averages for mutability with large error bars in recent times evidencing short
394 intervals indicating activity in a rather continuous way. In the case of zone B the recovery is still under way so it is
395 too soon to say anything at this time. Generally speaking we can observe that mutability values were high and their
396 error bars were small just before a major earthquake in zones A, B, and D.

397 Semestral averages for intervals between consecutive seisms and their corresponding error bars are very different
398 among the different regions. Both values decrease during the aftershock regime but no clear trend could be found
399 prior to a large earthquake.



400 As for the Calm zone C the mutability semestral averages are clearly increasing reaching 1.8 with narrowing error
401 bars. Although each zone can have different thresholds for triggering of a major event, such value or slightly lower
402 ones have been present just before large earthquakes in the other zones. Eventually zone C is showing a behavior that
403 should be further studied at the expectation of future large quakes.

404 Let us close by answering the 5 points raised in the introduction thus summarizing previous discussions and
405 conclusions. 1) Both Shannon entropy and mutability give similar responses to a major earthquake and its immediate
406 aftershock period, however they are independent and non-correlated during the quieter periods. 2) Shannon entropy
407 deals with the distribution as a whole while mutability deals with a sequential distribution of intervals of natural time;
408 this allows to the latter be more effective in providing larger contrasts if the values of the characteristics parameters. 3)
409 The recovery time and background activity are very well characterized by mutability allowing to discriminate among
410 different zones. 4) The mutability semestral averages reflect the seismic activity of the different zones indicating where
411 the subduction is relatively fluent or where the process could be stuck. 5) A combined analysis points to zone A as
412 stuck for many years and zone C slowly decreasing fluency in the subduction process which can be indication for
413 accumulation of energy in this zone.

414 This paper deals with the analysis of an important, but particular, seismic zone, namely the Nazca-South American
415 subduction front. Our results show that the use of mutability and Shannon entropy may distinguish the different
416 dynamics within this trench, and, specially, the fact that mutability may give a clue on the recovery time in a
417 given region between major earthquakes. Certainly, further studies should be made in order to establish the general
418 applicability of this approach, both by studying other seismic zones, and artificial catalogs, such as those given by
419 the ETAS model. We expect to develop this in future publications.



APPENDIX

In this appendix we provide examples of the way mutability if calculated following Eq. (3) for time sequences similar to those found in this problem, using $\nu = 24$ as it is done dynamically in previous presentation. Each column in Table IV lists one of these sequences representing intervals between consecutive seisms in minutes. First column, called "Even", is monotonic assigning one-hour interval evenly. Second column, called "Converging", is constructed by means of two intercalated sequences: one ascending and the other descending, so correlations are diluted. Third column, called Random, is formed by a randomly generated sequence. Fourth column, called Sequential, is formed by a monotonic increase of the intervals so it is highly correlated. As is can be readily found all columns average around 60 minutes between consecutive registers.

i	Even	Converging	Random	Sequential
1	60	30	57	48
2	60	90	112	49
3	60	32	9	50
4	60	88	49	51
5	60	34	60	52
6	60	86	73	53
7	60	36	14	54
8	60	84	112	55
9	60	38	9	56
10	60	82	49	57
11	60	40	90	58
12	60	80	40	59
13	60	42	55	60
14	60	78	49	61
15	60	44	67	62
16	60	76	35	63
17	60	46	87	64
18	60	74	67	65
19	60	48	67	66
20	60	72	49	67
21	60	50	21	68
22	60	70	77	59
23	60	52	38	60
24	60	68	108	61
μ	0.1875	1.2347	1.5670	0.3854

TABLE IV. Example of 4 time sequences (second to fifth columns) averaging 60 minutes between consecutive events. Mutability values for each column are given in the last row. The first column lists the sequence.

Results for the mutability of each column are given in the last row. As it could have been anticipated the Even sequence has the least information leading to the lowest mutability value. Next is Sequential, which reflects a monotonic increase in the time intervals. Notoriously higher is Converging where correlations are poor. The highest mutability value is for the Random sequence in spite a few values are repeated; if no repetitions are present and/or the interval span is higher the mutability value would be even larger.

It can be noticed that even in a 24-instant sequence mutability values can span an order of magnitude, This is even more so for real interevent sequences where intervals can reach several hours (a thousand minutes or more) thus differentiating behaviors of seismic activity.



ACKNOWLEDGEMENTS

437
438 One of us (EEV) is grateful to Fondecyt (Chile) under contract 1190036, and Center for the Development of
439 Nanoscience and Nanotechnology (CEDENNA) funded by Conicyt (Chile) under contract FB0807 for partial sup-
440 port. DP thanks Advanced Mining Technology Center (AMTC) and the Fondecyt grant 11160452. VM thanks
441 Fondecyt project 1161711, RAM acknowledges support from FAPDF (Brazil).
442

V. REFERENCES

- 444 Altamimi Z., Collilieux X., Legrand J., Garayt B., Boucher C.: A new release of the International Terrestrial Refer-
445 ence Frame based on time series of station positions and Earth Orientation Parameters, *J. Geophys. Research* 112,
446 B09401, 2007.
- 447
448 de Arcangelis L., Godano C., Grasso J.R., Lippiello E.: Statistical physics approach to earthquake occurrence and
449 forecasting, *Phys. Rep.* 628, 1-91, 2016.
- 450
451 Bressan G., Barnaba C., Gentili S., Rossi G.: Information entropy of earthquake populations in northeastern Italy
452 and western Slovenia, *Phys. Earth Planet. Interiors*, 271, 29-46, 2017.
- 453
454 Cakmur R.V., Egolf D.A., Plapp B.B., Bodenschatz E.: Bistability and competition of spatiotemporal chaotic and
455 fixed point attractors in Rayleigh-Bénard convection, *Phys. Rev. Lett.*, 79, 1853-1856, 1997.
- 456
457 Chian A. C.-L., Miranda R.A., Rempel E.L., Saiki Y., and Yamada M.: Amplitude-phase synchronization at the onset
458 of permanent spatiotemporal chaos, *Phys. Rev. Lett.*, 104, 254102, 2010.
- 459
460 Contreras D.J., Vogel E.E., Saravia G., Stockins B.: Derivation of a Measure of Systolic Blood Pressure Mutability: A
461 Novel Information Theory-Based Metric from Ambulatory Blood Pressure Tests, *J. American Soc. Of Hypertension*,
462 10, 217-223, 2016.
- 463
464 Cordaro E.G., Venegas P., Laroze D.: Latitudinal variation rate of geomagnetic cutoff rigidity in the active Chilean
465 convergent margin, *Annales Geophysicae*, 36, 275-285, 2018.
- 466
467 Cortez V., Saravia G., Vogel E.E., Phase diagram and reentrance for the 3D Edwards-Anderson model using informa-
468 tion theory, *J. Magn. Magn. Mater.* 372, 173-180, 2014.
- 469
470 Cover T.M., Thomas J.A.: *Elements of Information Theory*, John Wiley & Sons, New York, 2nd Ed., 2006
- 471
472 Crisanti A., Falcioni M., Paladin G., Serva M., A. Vulpiani A.: Complexity in quantum systems, *Phys. Rev. E*, 50,
473 1959-1967, 1994.
- 474
475 Klein E., Duputel Z., Zigioni D., Vigny C., Boy J.P., Doubre C., Meneses G.: Deep Transient Slow Slip Detected by
476 Survey GPS in the Region of Atacama, Chile, *Geophysical Research Letters*, 45, 12263-12273, 2018.
- 477
478 Lippiello E., Corral A., Bottiglieri M., Godano C., de Arcangelis L.: Scaling behavior of the intertime distribution:
479 Influence of large shocks and time scale in the Omori law, *Phys. Rev. E*, 86, 086119, 2012.
- 480
481 Luenberg D.G.: *Information Science*, Princeton University Press, Princeton N.J., 2nd Ed., 2006.
- 482
483 Manshour P., Saberi S., Sahimi M., Peinke J., Pacheco A.F., Reza Rahimi Tabar M.: Turbulencelike behavior of
484 seismic time series, *Phys. Rev. Lett.*, 102, 014101, 2009.
- 485
486 Métois M., Socquet A., Vigny C.: Interseismic coupling, segmentation and mechanical behavior of the central Chile
487 subduction zone, *J. Geophys. Research*, 117, B03406, 2012.
- 488
489 Métois M., Socquet A., Vigny C., Carrizo D., S. Peyrat S., Delorme A., Maureira E., Valderas-Bermejo M.-C., I.
490 Ortega I.: Revisiting the North Chile seismic gap segmentation using GPS-derived interseismic coupling, *Geophysical*



- 491 Journal International, 194, 1283-1294, 2013.
492
- 493 Miranda R.A., Rempel E.L., Chian A.C.-L.: On-off intermittency and amplitude-phase synchronization in Keplerian
494 shear flows, *Mon. Not. Royal Astron. Soc.*, 448, 804-813, 2015.
495
- 496 Nicolis O., Mateu J.: 2D Anisotropic wavelet entropy with an application to earthquakes in Chile, *Entropy*, 17,
497 4155-4172, 2015.
498
- 499 Roederer J.G.: *Information and its role in Nature*, Springer, Heidelberg, 2nd Ed., 2005.
500
- 501 Rundle J.B., Luginbuhl M., Giguere A., Turcotte D.L.: Natural Time, Nowcasting and the Physics of Earthquakes:
502 Estimation of Seismic Risk to Global Megacities, *Pure and Applied Geophysics* 175, 647-660, 2018.
503
- 504 Rundle J.B., Giguere A., Turcotte D.L., Crutchfield J.P., Donnellan A.: Global Seismic Nowcasting With Shannon
505 Information Entropy, *Earth and Space Science* 6 (1), 191-197, 2019.
506
- 507 De Santis A., Cianchini G., Favali P., Beranzoli L., Boschi E.: The Gutenberg-Richter law and entropy of earthquakes:
508 Two case studies in central Italy, *Bulletin Seism. Soc. America*, 101, 1386-1395, 2011.
509
- 510 Sarlis N.V., Skordas E.S., Varotsos P.A., Nagao T., Kamogawa M., Tanaka H., and Uyeda S.: Minimum of the
511 order parameter fluctuations of seismicity before major earthquakes in Japan, *Proceedings of the National Academy*
512 *of Sciences of the United States of America*, Vol.110, 1373413738, 2013.
513
- 514 Sarlis N.V., Skordas E.S., Varotsos P.A., Nagao T., Kamogawa M., and Uyeda S.: Spatiotemporal variations of
515 seismicity before major earthquakes in the Japanese area and their relation with the epicentral locations, *Proceedings*
516 *of the National Academy of Sciences of the United States of America*, Vol.112, 986989, 2015.
517
- 518 Sarlis N.V., Skordas E.S., Mintzelas A., and Papadopoulou K.A.: Micro-scale, mid-scale, and macro-scale in global
519 seismicity identified by empirical mode decomposition and their multifractal characteristics, *Scientific Reports*, Vol.
520 8, 9206, 2018.
521
- 522 Sarlis N.V., Skordas E.S., and Varotsos P.A.: A remarkable change of the entropy of seismicity in natural time under
523 time reversal before the super-giant M9 Tohoku earthquake on 11 March 2011, *EPL*, Vol. 124, 29001(7), 2018.
524
- 525 Sarlis N.V., Varotsos P.A., Skordas E.S., Uyeda S., Zlotnicki J., Nagao T., Rybin A., Lazaridou-Varotsos M.S., and
526 Papadopoulou K.A.: Seismic Electric Signals in seismic prone areas, *Earthquake Science*, Vol. 31 (2018), 44-51, DOI
527 10.29382/eqs-2018-0005-5.
528
- 529 Shannon C.E.: A mathematical theory of communication, *Bell. Sys. Tech. J.*, 27, 379-423, 1948
530
- 531 Telesca L., Lapenna V., Lovallo M.: Information entropy analysis of seismicity of Umbria-Marche region, *Natural*
532 *Hazards Earth Sys. Sci.*, 4, 691-695, 2004.
533
- 534 Telesca L., Lovallo M., Mohamed A.E.-E.A., ElGabry M., El-hady S., Abou Elenean K.M., ElBary R.E.F.: Infor-
535 mational analysis of seismic sequences by applying the Fisher Information Measure and the Shannon entropy: An
536 application to the 2004-2010 seismicity of Aswan area (Egypt), *Physica A*, 391, 2889-2897, 2012.
537
- 538 Telesca L., Lovallo M., Chamoli A., Dimri V.P., Srivastava K.: Fisher-Shannon analysis of seismograms of tsunami-
539 genic and non-tsunami-genic earthquakes, *Physica A*, 392, 3424-3429, 2013.
540
- 541 Telesca L., Lovallo M., Romano G., Konstantinou K.I., Hsu H.-L., Chen C.-C.: Using the informational Fisher-
542 Shannon method to investigate the influence of long-term deformation processes on geoelectrical signals: An example
543 from the Taiwan orogeny, *Physica A*, 414, 340-351, 2014.
544
- 545 Vallianatos F., Papadakis G., Michas G.: Generalized statistical mechanics approaches to earthquakes and tectonics,
546 *Proc. R. Soc. A*, 472, 20160497, 2016.
547



- 548 Varotsos P. and Alexopoulos K.: Physical properties of the variations of the electricfield of the earth preceding
549 earthquakes, I. Tectonophysics 110, 73-98, 1984.
550
- 551 Varotsos P. and Alexopoulos K.: Physical properties of the variations of the electricfield of the earth preceding
552 earthquakes, II. Determination of epicenter and magnitude, Tectonophysics 110, 99-125, 1984.
553
- 554 Varotsos P., Alexopoulos K., Nomicos K. and Lazaridou M.: Earthquake prediction and electric signals, Nature 322,
555 120, 1986.
556
- 557 Varotsos P. and Lazaridou M.: Latest aspects of earthquake Prediction in Greece based on Seismic Electric Signals.
558 I, Tectonophysics 188, 321-347, 1991.
559
- 560 Varotsos P., Alexopoulos K. and Lazaridou M.: Latest aspects of earthquake prediction in Greece based on Seismic
561 Electric Signals II, Tectonophysics 224, 1-37 1993.
562
- 563 Varotsos P.: The Physics of Seismic Electric Signals, TerraPub, Tokyo (2005) 338pages.
564
- 565 Varotsos P.A., Sarlis N.V. and Skordas E.S.: Phenomena preceding major earth-quakes interconnected through a
566 physical model, Annales Geophysicae 37, 315-324, 2019.
567
- 568 Varotsos P.A., Sarlis N.V., Skordas E.S., Uyeda S. and Kamogawa M.: Natural time analysis of critical phenomena,
569 Proceedings of the National Academy of Sciences of the United States of America, Vol.108 (2011), 11361-11364.
570
- 571 Venegas-Aravena P., Cordaro E.G., Laroze D.: A review and upgrade of the lithospheric dynamics in context of the
572 seismo-electromagnetic theory, Natural hazards and earth system sciences, 19, 1639-1651, 2019.
573
- 574 Vogel E.E., Saravia G., Pasten D., Munoz V.: Time-series analysis of earthquake sequences by means of information
575 recognizer, Tectonophysics, 712, 723-728, 2017.
576
- 577 Vogel, E.E., and Saravia, G., and Ramirez-Pastor, A.J.: Phase diagrams in a system of long rods on two-dimensional
578 lattices by means of information theory, Phys. Rev. E, 96, 062133, 2017.
579
- 580 Vogel E.E., Saravia G., Bachmann F., Fierro B., Fischer J.: Phase Transitions in Edwards-Anderson Model by Means
581 of Information Theory, Physica A, 388, 4075-4082, 2009.
582
- 583 Vogel E.E., Saravia G., Cortez L.V.: Data Compressor Designed to Improve Recognition of Magnetic Phases, Physica
584 A, 391, 1591-1601, 2012.
585
- 586 Vogel E.E., Saravia G.: Information Theory Applied to Econophysics: Stock Market Behaviors, European J. of Physics
587 B, 87, 1-15, 2014.
588
- 589 Vogel E.E., Saravia G., Astete J., Díaz J., F. Riadi F.: Information Theory as a Tool to Improve Individual Pensions:
590 The Chilean Case, Physica A, 424, 372-382, 2015.
591
- 592 Vogel E.E., Saravia G., Kobe S., Schumann R., Schuster R.: A Novel Method to Optimize Electricity Generation
593 from Wind Energy, Renewable Energy, 126, 724-735, 2018.
594
- 595 Xi H., Gunton J.D.: Spatiotemporal chaos in a model of Rayleigh-Bénard convection, Phys. Rev. E, 52, 4963-4975,
596 1995.
597
- 598 Zhang Y., Meng Q.Y.: A statistical analysis of TIR anomalies extracted by RSTs in relation to an earthquake in the
599 Sichuan area using MODIS LST data, Natural hazards and earth system sciences, 19, 535-549, 2019.
600
- 601 Web site of Servicio Sismológico Nacional (Chile), <http://ssn.dgf.uchile.cl/>, 2019.